Supporting Information to "Charge blinking statistics of semiconductor nanocrystals revealed by carbon nanotube single charge sensors"

Ewa Zbydniewska,[†,‡] Anna Duzynska,[‡] Michka Popoff,[†,¶] Djamila Hourlier,[†] Stéphane Lenfant,[†] Jaroslaw Judek,[‡] Mariusz Zdrojek,[‡] and Thierry Mélin[*,†]

Institute of Electronics Microelectronics and Nanotechnology, IEMN-CNRS UMR 8520, Avenue Poincaré CS60069, 59652 Villeneuve d'Ascq, France, Faculty of Physics, Warsaw University of Technology, Koszykowa 75, 00-662 Warsaw, Poland, and Lille Centre for Infection and Immunity, Cellular Microbiology of Infectious Pathogens, CNRS UMR8204, INSERM U1019, University of Lille Nord-de-France, Institut Pasteur de Lille, F-59019 Lille, France

E-mail: thierry.melin@univ-lille1.fr

Abstract

We here provide supporting information about the device fabrication, fluorescence blinking experiments, as well as the determination of the charging energy E_c for Device B.

[*]To whom correspondence should be addressed

[†]Institute of Electronics Microelectronics and Nanotechnology, IEMN-CNRS UMR 8520, Avenue Poincaré CS60069, 59652 Villeneuve d'Ascq, France

[‡]Faculty of Physics, Warsaw University of Technology, Koszykowa 75, 00-662 Warsaw, Poland

[¶]Lille Centre for Infection and Immunity, Cellular Microbiology of Infectious Pathogens, CNRS UMR8204, INSERM U1019, University of Lille Nord-de-France, Institut Pasteur de Lille, F-59019 Lille, France

Device fabrication

In the case of Device A, carbon nanotubes were directly grown by chemical vapour deposition performed using methane (purity 99.999%) on a 1 μm thick thermally grown SiO_2 substrate with a previously prepared catalyst, using the following ingredients (from Sigma Aldrich): 80 mg of $Fe(NO_3)_3 \cdot 9H_2O$, 4 mg of bis(acetylacetonato)-dioxomolybdenum(VI), 60 mg of aluminium oxide, all in 60 mL of methanol (HPLC). All the components were mixed together and ultrasonicated for 1 h before use. 10 μl of the catalyst solution was dropped onto the substrate and dried with a nitrogen stream. Samples were introduced into the furnace immediately after catalyst deposition. Alignment marks were defined by EBL after the CNT growth, followed by the location of the nanotube and the fabrication of Ti (5 nm) / Au (45 nm) electrodes connecting individual nanotubes. Electrical measurements were used to discriminate between semiconducting and metallic nanotubes. CdSe/ZnS NCs with a measured diameter of 4 nm and an absorption peak at 500 nm were purchased from MKNano (product reference MKN-CdSe/ZnS-T500) ; they were deposited by being drop-cast from the as-received colloidal dispersion in toluen.

In the case of Device B, 99 % pure semiconducting single-walled carbon nanotubes purchased in powder form from NanoIntegris were horn-sonicated in 1,2-dichlorobenzene and subsequently deposited by being drop-cast onto Si/SiO_2 samples (300 nm thick thermally grown silicon dioxide from a p^+ doped silicon wafer) pre-patterned with alignment marks defined by electron beam lithography (EBL). Individual nanotubes are then located with respect to alignment marks using AFM, followed by the alignment by EBL of Ti (5 nm) / Au (45 nm) electrodes. Fabricated NC-CNTFET devices were characterized by AFM and by standard $I_{DS}(V_{GS})$ electrical measurements prior to NC deposition. Electrical measurements were performed in a homemade shielded probe station with triaxial connection cables to ensure a minimum of electrical noise. The power spectra of current time traces were obtained numerically starting from the real-time experimental data. AFM images were acquired using an ambient-air AFM (Dimension 3100, Brüker Nano) and standard doped-silicon AFM tips. CdSe/ZnS NCs with an experimental diameter of 5 nm and an absorption peak at 620 nm were purchased from MKNano (product reference MKN-CdSe/ZnS-

T620); these NCs were deposited using the same technique used to fabricate Device A. AFM was used to ensure for the presence of single or few NCs along the nanotubes.

Fluorescence experiments

The optical blinking of the colloidal nanocrystals was verified in two environments: on SiO_2 and on carbon nanotubes. The first sample consisted of 6 nm CdSe/ZnZ NCs deposited onto a SiO_2 layer, whereas the second sample consisted of 4 nm CdSe/ZnZ NCs deposited onto a NanoIntegris carbon nanotube carpet (the fabrication details are available elsewhere[1]). A sketch of the two samples is shown in Figure 1a and d.

Optical images were acquired on a Zeiss Elyra P1 inverted optical microscope equipped with a high-speed EMCCD Andor Xion camera (Ref. DU-897D-CSO-#BV-461). We used a Zeiss Alpha Plan-Apochromat 100x/1.46 Oil DIC M27 Elyra (420792-9800-720) objective. The microscope was operated in epifluorescence mode using a 1.6$\times$ magnifying lens. The acquisition software was Zen 2011 SP2 (black edition) (64-bit) Release 8.0.7.273, Configuration 7.00.00. The samples were placed on glass-bottom dishes (WillCo-dish, WillCo Wells B.V.) and imaged at room temperature. For each sample, more than 400 frames were acquired. The wavelength of the excitation laser was 561 nm (although excitation could also be achieved with a laser at 488 nm). A long-pass filter (Zeiss LP570) was used to filter the excitation light and to collect the photons emitted by the blinking dots. The exposure time was 6 ms for the first sample (with a reduced image size of 64$\times$64 pixels) and 40 ms for the second sample (512$\times$512 pixels). The NC blinking is illustrated from a set of three fluorescence images (Figure 1b and e for the first and second samples, respectively). The image analysis was performed using ImageJ software (http://imagej.nih.gov/ij/). The mean intensity of a dot was extracted using the particle detection algorithm on a region of interest for each frame. An illustration of the recorded fluorescence time traces is shown in Figure 1c and f.

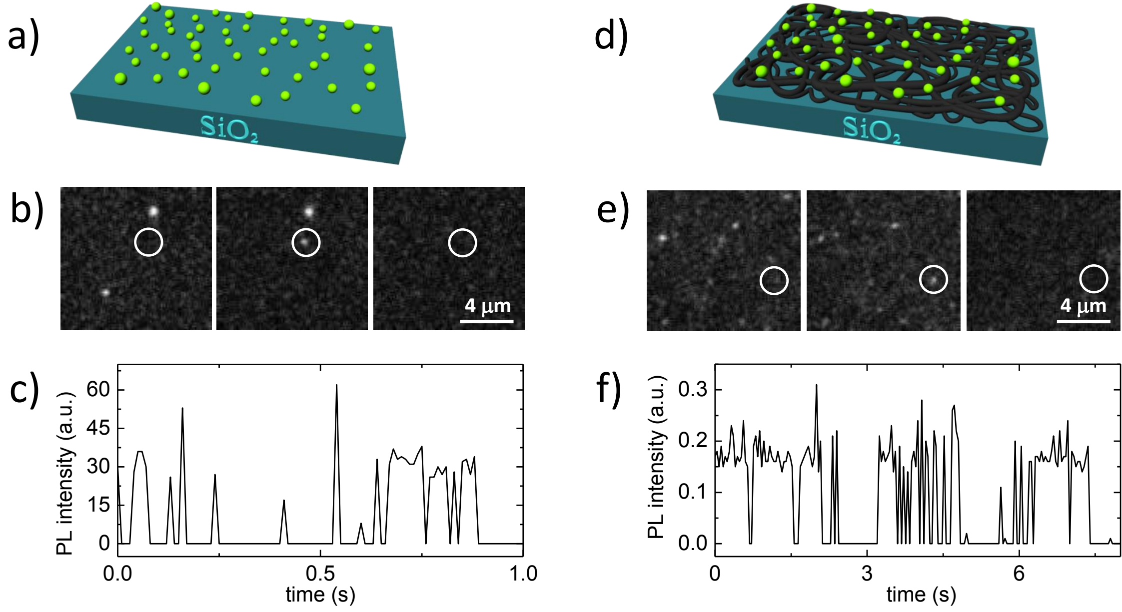

Figure 1: Schematics of the samples used for fluorescence experiments, with a) 6 nm CdSe/ZnS NCs deposited onto SiO_2 and b) 4 nm CdSe/ZnS NCs deposited onto a NanoIntegris nanotube carpet. b) and e) Fluorescence images showing the NC blinking (a highlighted NC is shown in each case for sake of illustration). c) and f) Examples of fluorescence time traces for each sample.

Determination of the charging energy E_c for Device B

We here determine the charging energy E_c for Device B, as a supporting information to the main paper. The same methodology is applied to this Device as compared to Device A. We show histograms of the current traces in Figure 2 for V_{DS}=150 mV (top) and V_{GS} varied by steps of 1 V. The data are shown in the V_{GS} range for which RTS could be observed under the measurement conditions. We used a recording bin time τ_{min} = 0.1 ms and total recording time τ_{max}=1 s. For each V_{GS} value, the drain bias was switched to V_{DS} = 300 mV; the corresponding data are shown in Figure 2 (bottom). The behaviour of Device B differs substantially from that of Device A because the histograms appear as strongly peaked on the L peak only for V_{DS} = 150 mV, irrespective of the back-gate bias V_{GS}. However, the histograms are strongly peaked on the H peak for V_{DS} = 300 mV. In both cases, the back-gate action is almost insignificant, which suggests a non-equilibrium population of the electronic state responsible for the observed RTS. The analysis using Eq. (1) of

the main paper should therefore be handled with care. However, as shown in Table 1, we computed the same data as for Device A to determine the effective charging energy at hand in the blinking process observed in Device B. The results show values of $2|E_T - E_F|$ in the 120-200 meV range. Similarly as for Device A, we also estimated the back-gate voltage shift $\Delta V_{GS}(L-H)$ corresponding to the jump in current levels between the H and L states from the device transfer characteristics $I_{DS}(V_{GS})$ obtained for $V_{DS} = 150$ mV (data from Figure 2 of the main paper) or $V_{DS} = 300$ mV (data not shown). This analysis provides an average value for $\Delta V_{GS}(L-H)$ of $\approx$ 670 mV. However, to interpret this value in terms of the NC charging energy, we need to use a lever arm β' (not β) because of the smaller oxide thickness (300 nm for Device B compared to 1 μm for Device A). In the absence of existing data in the literature for this device geometry, we compute β' as a function of β : $\beta' = (C_A/C_B)\ \beta$, where C_A and C_B refer to the nanotube / back-gate capacitance for Devices A and B, respectively. We thus obtain $\beta' = \beta/(1.25 \pm 0.1)$ =2.95 $\pm$ 0.25 (using a measured nanotube diameters of 2 nm and 3 $\pm$1 nm, respectively, for Devices A and B), which gives the measured charging energy $e\Delta V_{GS}/\beta'$ listed in Table 1. An average charging energy $E_c \approx$ 225 meV can be deduced, which satisfies $E_c \geq 2|E_T - E_F|_{max}$.

We therefore obtain a similar picture as for Device A, where the RTS can be understood as the charging of a trap with charging energy in the $\approx$ 200 meV range. However, the trap charging here is not activated by the device back-gate bias V_{GS} but rather by a change of V_{DS}. We attribute this behaviour to an out-of-equilibrium trap state population, in contrast with Device A, whereas the observed change as a function of V_{DS} may tentatively be assigned to the trap charging by hot carriers from the CNTFET channel under increased V_{DS} values.

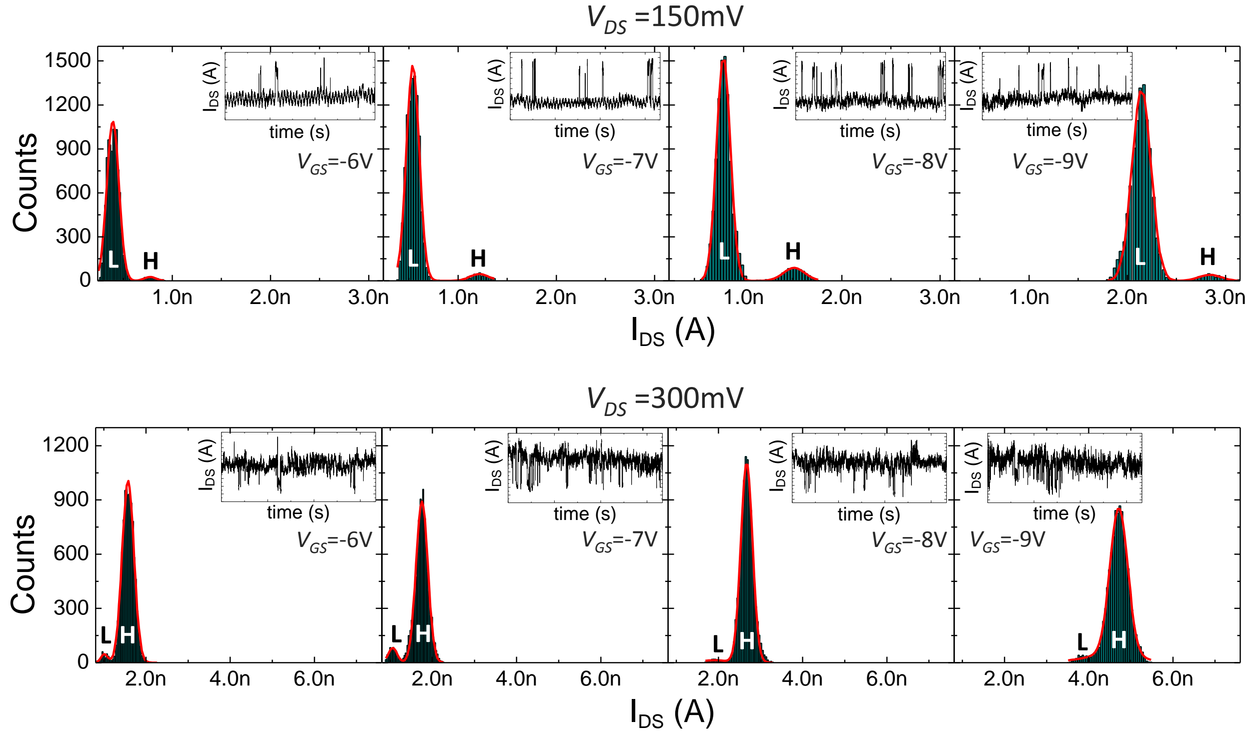

Figure 2: **RTS back-gate dependence for Device B.** Histograms of I_{DS} current levels recorded as a function of the back-gate bias V_{GS}, plotted (top) for a source drain bias V_{DS} = 150 mV and (bottom) for V_{DS} = 300 mV. The device current traces have been recorded for each plot using a recording bin time τ_{min} = 0.1 ms and a total recording time τ_{max} = 1 s. Insets illustrate the RTS of current traces over a 1 s duration.

References

(1) Duzynska, A., Judek, J. & Zdrojek, M. Temperature-dependent nonlinear phonon behavior in high-density carbon nanotube thin films. *Appl. Phys. Lett.* **105**, 213105 (2014).

Table 1: **Analysis of the RTS in Device B.** The tables refer to V_{DS} =150 mV (top) and V_{DS} = 300 mV (bottom). The table shows the operation back-gate bias V_{GS}, the ratio between the average times $< \tau_L >$ and $< \tau_H >$ (data from Figure 2) and the corresponding $E_T - E_F$ value, as derived from Eq. (1) in the main paper(see text); the back-gate voltage difference between the current levels associated with the L and H states (obtained from the transfer characteristics of Device B without NC in Figure 2 in the main paper) and the corresponding charging energy obtained using the lever arm β'=2.95 (see text).

V_{GS}	$< \tau_L > / < \tau_H >$	$2(E_T - E_F)$	$\Delta V_{GS}(L-H)$	$e\Delta V_{GS}(L-H)/\beta'$
-6 V	40	**190 meV**	0.48 V	**160 meV**
-7 V	22	**160 meV**	0.75 V	**250 meV**
-8 V	11	**126 meV**	0.82 V	**280 meV**
-9 V	82	**172 meV**	0.77 V	**260 meV**
-6 V	0.042	**- 164 meV**	0.55 V	**185 meV**
-7 V	0.079	**- 132 meV**	0.60 V	**200 meV**
-8 V	0.020	**- 200 meV**	0.62 V	**210 meV**
-9 V	0.066	**-140 meV**	0.79 V	**270 meV**